Hindawi
Adsorption Science & Technology
Volume 2023, Article ID 7073318, 13 pages
https://doi.org/10.1155/2023/7073318

Research Article

Surface Diffusion of C_1–C_3 Alcohols on Multiwall Carbon Nanotubes

Alexey Zhokh, Tamila Serebrii, and Peter Strizhak

L.V. Pisarzhevskii Institute of Physical Chemistry, National Academy of Sciences of Ukraine, Prospekt Nauki, 31, Kyiv 03028, Ukraine

Correspondence should be addressed to Alexey Zhokh; al.zhokh@gmail.com

Received 4 December 2022; Revised 13 February 2023; Accepted 23 August 2023; Published 2 September 2023

Academic Editor: Stefano Salvestrini

The diffusion of methanol, ethanol, and 2-propanol using individual multiwall carbon nanotubes (MWCNT) and MWCNT bundles was investigated for the first time via application of the quartz crystal microbalance. At small times, the release of alcohol obeys the advective mechanism. In contrast, no deviations from Fick's law were justified at large times. This situation holds for either individual MWCNTs or MWCNT bundles. The utilized MWCNTs are mainly closed from both ends. Therefore, the alcohol release is controlled by surface diffusion. The measured surface diffusivity is in the order of 10^{-13} m^2/s. The obtained diffusivities are in close proximity with the known surface diffusion coefficients on carbon materials.

1. Introduction

Carbon nanotubes (CNTs) attract much interest due to their unique properties. The CNTs typically exhibit good electrical conductivity [1], high elasticity, [2], and exceptional thermal conductivity [3]. In addition, the multiwall carbon nanotubes (MWCNTs) are characterized by extremely high tensile strength [4]. These properties allow the CNT application in various fields, e.g., in biomedicine and biotechnology [5, 6]; energy storage; for the production of lithium-ion batteries, supercapacitors, transistors, and sensors; and new composite materials [7, 8]. CNTs are often used as an essential part of composite membranes for gas separation and water purification [9], even though the CNTs are likely not to be directly involved in the separation process [10]. The CNTs may be also used as effective sorbents for the removal of heavy metal ions [11, 12], polycyclic aromatic hydrocarbons [13], pesticides [14], and other chemicals in analytical chemistry [15]. Moreover, the CNTs are extensively used as catalysts in photo- and electrocatalysis [16]. In the field of heterogeneous catalysis, the CNTs serve either as a catalyst support [17] or as a heterogeneous catalyst, e.g., for oxidative dehydrogenation of ethylbenzene [18], alcohol conversion [19], and ethylene hydrogenation [20].

The absence or insignificance of the diffusion limitations is a key feature of a material used as either an effective sorbent or a catalyst. Quite a lot of studies in both theoretical and experimental fields are focused on the investigation of the diffusion peculiarities in the CNTs. Different diffusion regimes were verified for diffusive transport through CNTs. In particular, the hydrogen transport in the CNTs with the inner diameter of 1.1 nm follows the single-file, standard, and ballistic diffusion regimes. The transition between the regimes is associated with the Knudsen number [21]. The results of the molecular simulations outlined that the diffusion regime crosses over from the single file to the standard Fickian in the case if the inner CNT diameter reaches 1.0 nm [22]. In addition, the diffusion regime in different regions of the CNTs was found to differ significantly. For CNTs with a large diameter, the ballistic diffusion was identified near the CNT wall changing to the Fickian diffusion in the center of the CNTs [23]. The multicomponent diffusion of H_2 and C_1–C_4 alkanes in the CNTs was found to be predicted by the Maxwell-Stefan diffusion model in a concise manner [24]. A study on the methane diffusion rates in nanoporous carbon and CNTs revealed that the diffusion in constricted CNTs is an order of magnitude slower compared to nanoporous carbon [25]. The self-diffusion coefficient of SO_2 in

the CNTs studied employing molecular simulations increases with the temperature increase and reduces with the CNT diameter increase [26]. The transport diffusion coefficient in deformed CNTs was identified as a function of the deformation factor [27].

The intriguing and sometimes controversial results were obtained on the water transport in CNTs. On the one hand, it was concluded that the water diffusion mechanism follows ballistic dynamics [28]. On the other hand, the subdiffusive behavior of the mean square displacement of the water molecules in the single-wall CNTs has been observed by neutron spin echo monitoring [29]. The diffusion coefficient of H_2O exhibits an anomalous significant increase with the increase of the inner diameter of CNTs [30]. The enhancement of the H_2O transport in CNTs is attributed to the change of the hydrogen bond number [31]. Similar to water, ionic liquids exhibit ultrafast diffusion in CNTs due to the complex interplay of friction forces, stacking, molecular size, and cooperative dynamic interactions [32].

On an experimental basis, the investigation of the diffusion and adsorption in CNTs is performed using nuclear magnetic resonance spectroscopy [33, 34], neutron scattering [35], and quartz crystal microbalance (QCM) techniques [36]. The use of the CNT-based QCM sensors for quantitative measurements of various chemicals, e.g., humidity [37] or volatile organic compounds [38], is a convenient approach due to the fact that the QCM covered with CNTs gives a selective response [39], especially in combination with polymer coating [40, 41]. Additionally, the kinetics of the CNT release may be studied by the QCM method, e.g., from the silica surface [42]. In the current paper, we present the study on the release of C_1–C_3 alcohols from individual MWCNTs and the bundles of the MWCNTs using the QCM approach. Adsorption-desorption of C_1–C_3 alcohols on CNTs is the governing stage for fuel cells, selective sensors, separation, and purification [43–46]. For engineering purposes, an accurate description of the rate of the corresponding process is required. To the best of our knowledge, the desorption kinetics of methyl, ethyl, and isopropyl alcohol from the MWCNTs under the assumption of diffusion control is investigated for the first time. Quite a lot of studies are focused on the transport processes inside the open CNTs reporting the presence of various types of diffusion [47, 48], e.g., fast diffusion (due to high values of the diffusion coefficients), ballistic diffusion, and anomalous diffusion. The productivity of the engineering processes involving CNTs can be significantly improved by the high rate of alcohol transport. It is interesting to verify the existence of such transport on the outer surface of carbon nanotubes. To this end, the kinetics of the alcohols' release from the surface of the closed MWCNTs and their aggregates is investigated. The estimated diffusivities correspond to the surface diffusion coefficients for the carbon materials.

2. Experimental

2.1. MWCNT Synthesis and Characterization. The MWCNTs were prepared via ethylene decomposition over a Ni/CaO catalyst (Ni content was 20%). The detailed procedure of the MWCNT synthesis is provided in Ref. [49]. The as-prepared MWCNTs were treated with an HNO_3 aqueous solution (70% of HNO_3) for 2 hours to remove the catalyst and amorphous carbon. Afterward, the MWCNTs were washed with deionized water and dried at 433 K.

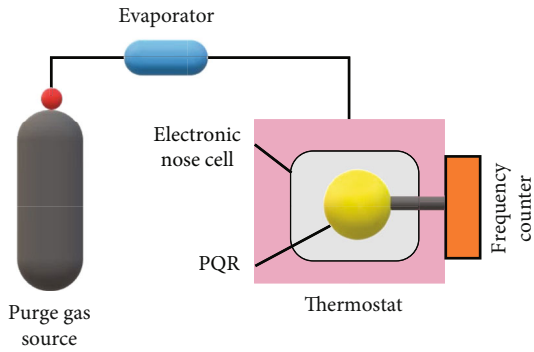

Figure 1: A sketch of the experimental instrument.

TEM microimages of the MWCNTs were recorded using the Selmi PEM-125 transmission electron microscope at the acceleration voltage of 100 kV. Nitrogen adsorption and desorption isotherms were obtained by the Sorptomatic-1990 instrument at the temperature of boiling liquid nitrogen (77 K). Additionally, the as-prepared MWCNTs were characterized by X-ray diffraction, scanning electron microscopy images, Fourier transform infrared spectroscopy, Raman spectroscopy, X-ray photoelectron spectroscopy, and Boehm titration. In detail, the properties of the MWCNTs used in this study are discussed in Refs. [20, 50].

2.2. QCM Study. A QCM setup is based on the electronic nose cell [51]. The piezoelectric quartz resonator (PQR) is installed inside the cell. The cell is located inside a thermostat to preserve the constant temperature during the measurements. The PQR is joined to the frequency counter. The latter is mounted on the outer side of the thermostat. The cell is purged with helium flow. A diffusant is injected into the cell through the evaporator for a gas chromatograph. An amount of alcohol was manually injected into the cell using the syringe for gas chromatography (Hamilton model 701, US). A sketch of the QCM instrument is depicted in Figure 1.

The PQRs (Ukrpiezo Ltd., Ukraine) with a fundamental frequency of 10 MHz and nickel-silver electrodes were coated with MWCNT bundles and individual MWCNTs. The MWCNT powder was suspended in 2-propanol. After 2 hours of sedimentation, the suspension was airbrushed to obtain the coated PQR. To derive the PQR coated with individual MWCNTs, the MWCNT suspension in 2-propanol was ultrasonicated using a Bandelin Sonopuls 4100 ultrasonic homogenizer equipped with TS106 horn for 30 minutes at 40% of maximum ultrasonic amplitude. Following ultrasonic treatment, the suspension was sedimented for 1 hour and airbrushed to coat the PQR. Simultaneously, the size of the MWCNT bundles and individual MWCNTs in the final suspension was controlled by TEM microimaging (Figure 2). The coating preparation procedure resulted in the PQR coating consisting of MWCNT bundles of approximately 4 μm in size (Figure 2(a)), whereas ultrasonic

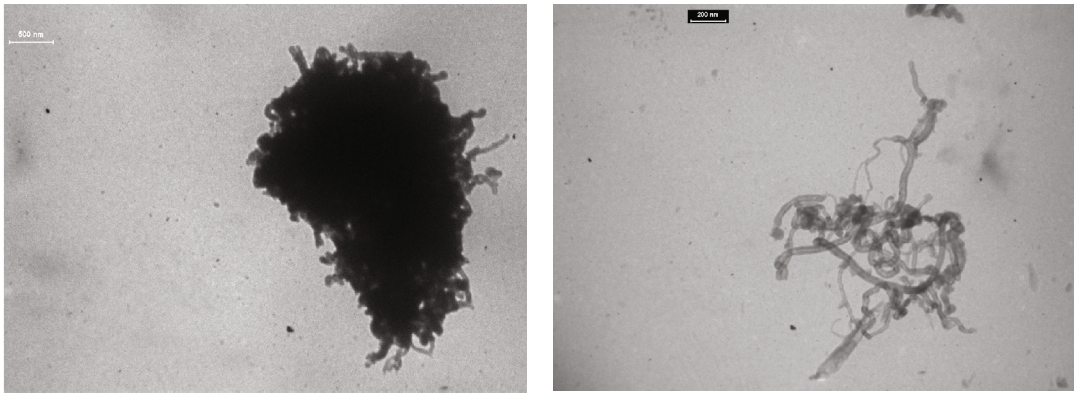

(a) (b)

Figure 2: Typical MWCNT bundle (a) and individual MWCNTs (b) used for PQR coating.

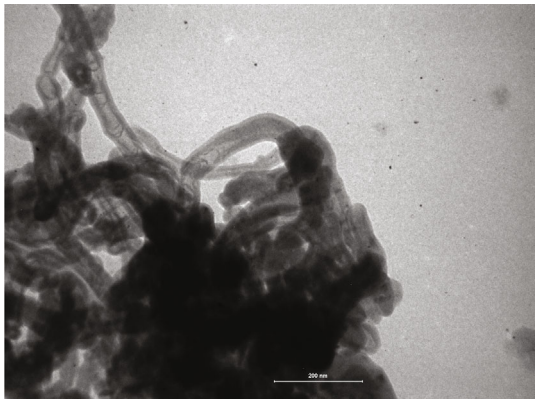

Figure 3: A typical TEM image of the MWCNTs.

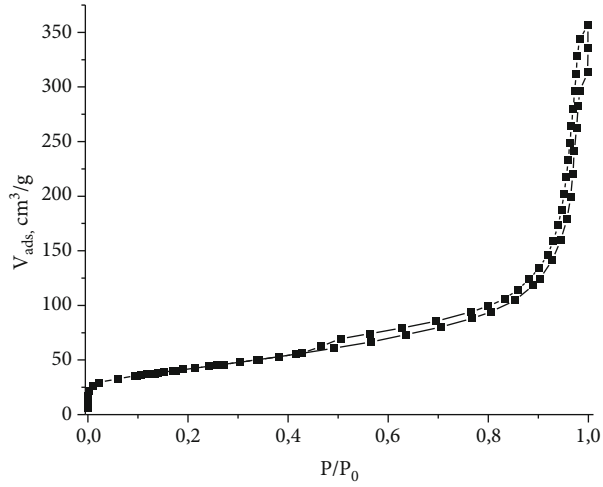

Figure 4: N_2 adsorption-desorption isotherm for the MWCNTs.

treatment yields in the PQR coated by a small network of individual MWCNTs (Figure 2(b)). The PQR loadings of approximately 3.0 kHz and 3.1 kHz were achieved for the MWCNT bundles and individual MWCNTs, respectively.

Methanol, ethanol, and 2-propanol (all 99.9% purity) were used as diffusing agents. The amount of each alcohol injected was 5 μl. The temperature inside the cell with PQR was kept at 345 K. The cell was purged with helium at a flow rate of 35 cm^3/min.

The alcohol amount adsorbed on the MWCNTs is related to the PQR frequency shift through the following expression:

$$M = \frac{\Delta f}{\Delta F}, \quad (1)$$

where M reflects an amount of the adsorbed alcohol (mg/g), Δf denotes the QCM frequency shift caused by the alcohol adsorption (Hz), and ΔF is a QCM frequency shift governed by the PQR coating with MWCNTs (kHz).

3. Results and Discussions

3.1. MWCNT Characteristics. The TEM image of the MWCNTs (Figure 3) reveals that they are predominantly cylindrical. Some CNTs are of bamboo-like morphology. Some CNTs are characterized by bends. The diameter of the CNTs varies between approximately 40 and 60 nm. The average thickness of the CNT walls is approximately 8 nm. The higher is the thickness of the CNT, the lower is the thickness of the CNT walls. This situation is associated with a higher number of defects in the structure of the CNTs with a smaller diameter.

The textural properties were estimated from the nitrogen adsorption-desorption isotherm (Figure 4). The hysteresis loop of the isotherm corresponds to type H3 which is convenient for the aggregates of platy particles [52], e.g., MWCNT bundles. According to the isotherm data, the pore volume (Gurvich) of the as-prepared MWCNTs is 0.48 cm^3/g, the BET surface area is 149 m^2/g, the median mesopore diameter (BJH) is 38 nm, and the mesopore surface area (t-plot) is 126 m^2/g. Almost no microporosity was observed. The median mesopore diameter obtained from the isotherm seems to be quite similar compared to the average inner diameter of the CNTs estimated from TEM data. However, the median mesopore diameter obtained from the isotherm is scarcely defined by the inner cavities inside CNTs. The

CNTs are either partially closed on the ends or partitioned, as follows from Figure 3. This supports the idea that the mesoporosity of the bundles is associated mainly with the spaces between the aggregated nanotubes in a bundle.

3.2. Mass Transfer Analysis

3.2.1. PQR Response Processing. A PQR response is obtained as a frequency shift change versus time for all alcohols (Figure 5). Ultrasonication considerably affects the frequency shift. The latter is almost 20% higher for the PQR coated by individual MWCNTs compared to the PQR coated by the MWCNT bundles. The PQR loadings are very similar for both coatings. Therefore, a higher amount of alcohol is absorbed by individual MWCNTs. Seemingly, alcohol molecules are adsorbed on the surface of MWCNTs. Individual MWCNTs exhibit almost no geometric constraints limiting the adsorption on the MWCNT surface. In an MWCNT bundle, the access of the alcohol molecules to the MWCNT surface is partially restricted by multiple contacts between nanotubes (Figure 2(a)).

The frequency shift is recalculated into the amount of the adsorbed alcohol evolving in time according to formula (1) (Figure 6). The adsorbed amounts are very similar for ethanol and 2-propanol, whereas methanol uptake is considerably lower. However, retention times are almost identical for methanol and ethanol. Mass release of 2-propanol is characterized by a higher retention time compared to that of methanol and ethanol. This situation seems to be convenient because the kinetic diameter and the molecular weight of the ethanol are lower than those of 2-propanol. In general, the smaller is the kinetic diameter and the molecular weight, the higher is the mobility of a molecule and, as a result, the diffusion rate.

3.2.2. Short-Time Analysis. The evolution of the alcohol concentration within the MWCNTs may be described by the second Fick's law of diffusion. Considering the one-dimensional diffusion, the relevant mathematical equation reads as follows:

$$\frac{\partial C}{\partial t} = D \bullet \frac{\partial^2 C}{\partial x^2}, \tag{2}$$

where C is the concentration (mole/m), t is the time (s), x is the spatial coordinate (m), and D denotes diffusivity (m^2/s). Equation (2) is used under the assumption that diffusivity is concentration-independent, i.e., it corresponds to the diffusion coefficient. The change of the alcohol mass registered by QCM may be approximated by the solution of equation (2) given in the following form [53]:

$$\frac{M(t)}{M_0} = 1 - \frac{2}{L} \bullet \sqrt{\frac{D}{\pi}} \bullet \sqrt{t}. \tag{3}$$

Here, $M(t)$ reflects an amount (mg/g) of alcohol adsorbed at time t (s), M_0 is the maximum adsorbed amount of alcohol which is observed at time $t = 0$ (mg/g), and L corresponds to the diffusion length (m). Equation (3) naturally represents a linear dependence of $1 - M(t)/M_0$ on $\sqrt{t}$ with the slope proportional to the diffusivity. Therefore, the diffusivity may be measured by simple linearization of the experimental QCM data in the $(1 - M(t)/M_0) - \sqrt{t}$ coordinates. Different ranges of the validity of equation (3) are presented in the literature. On the one hand, this equation is considered to be appropriate for the mass transfer description at "intermediate" times [54]. On the other hand, equation (3) is treated to give a good approximation in the range of $M(t)/M_0 > 0.5$, i.e., at small times [53]. In the current study, we apply equation (3) in the short and intermediate time ranges, i.e., for $M(t)/M_0 > 0.2$.

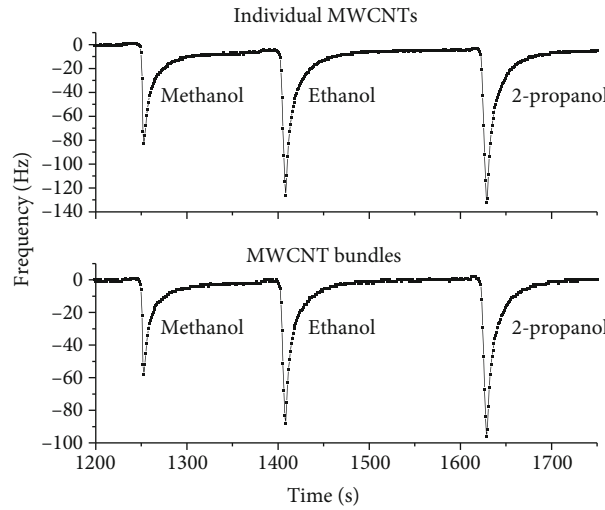

Figure 5: Frequency change versus time.

For the analysis of the experimental data based on equation (3), the amount of the adsorbed alcohol is recalculated into the normalized mass release $(1 - M(t)/M_0)$. Figure 7 presents the experimental data transformed into the normalized mass release versus the square root of time. Figure 7 accounts for the experimental data at small and intermediate times. From this figure, it is clear that the data points are not distributed along the straight line of the model. The experimental data do not exhibit a linear trend. The correspondence between the experimental data and the theoretical equation is rather poor. The results of the fitting procedures performed under equation (3) are presented in Table 1. In the literature, such divergence is sometimes treated as evidence of the anomalous diffusion mechanism [55, 56]. However, the inapplicability of Fick's law may be governed not only by the existence of the anomalous diffusion but also by the presence of the transport phenomena of nondiffusive origin, e.g., advection and rate-limiting adsorption.

The obtained results demonstrate that the standard diffusion equation fails at small times. The mass release is approximately a linear function of elapsed time at small times, according to Figure 6. A linear dependence corroborates that the alcohol outflows from the MWCNTs with constant velocity. Therefore, at small times, the driving

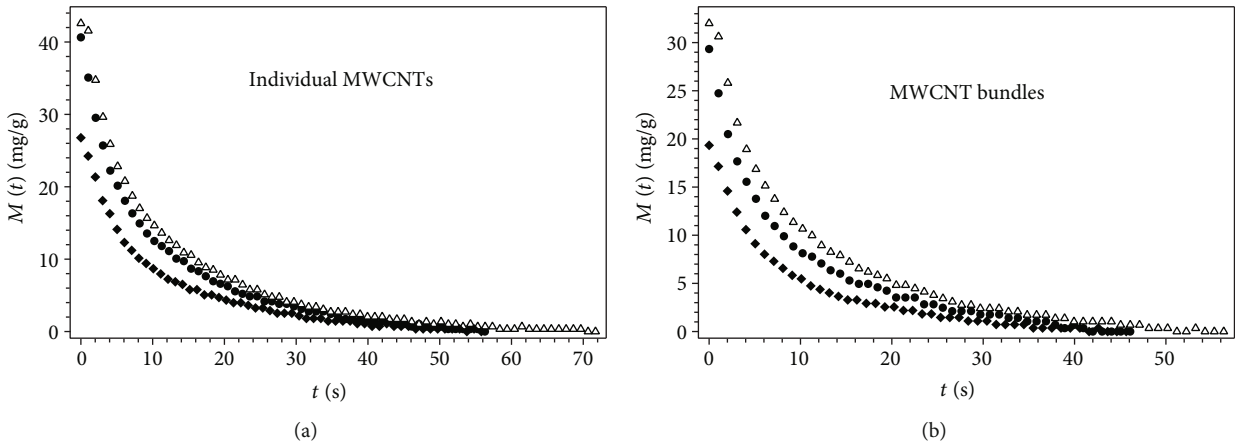

Figure 6: Methanol (◆), ethanol (●), and 2-propanol (△) mass release evolving in time for individual MWCNTs (a) and MWCNT bundles (b).

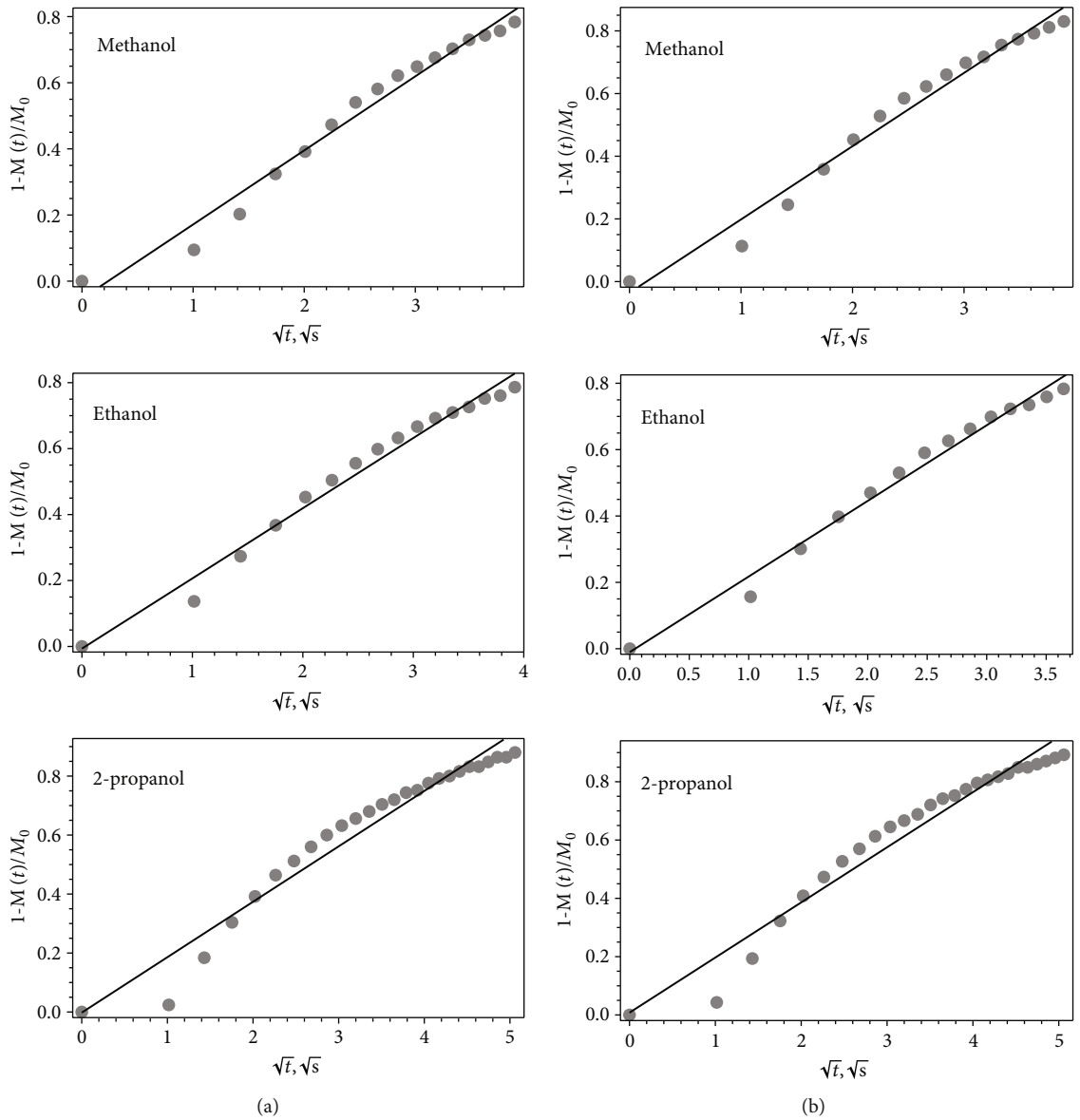

Figure 7: The normalized mass release plotted as a function of $\sqrt{t}$ (points) and best-fit line individual MWCNTs (a) and MWCNT bundles (b).

Table 1: Fitting results from Figure 7.

Figure	Alcohol	Fitted equation	R^2
Figure 7(a)	Methanol	$1 - \frac{M(t)}{M_0} = 0.22 \bullet \sqrt{t}$	0.976
	Ethanol	$1 - \frac{M(t)}{M_0} = 0.21 \bullet \sqrt{t}$	0.981
	2-Propanol	$1 - \frac{M(t)}{M_0} = 0.18 \bullet \sqrt{t}$	0.953
Figure 7(b)	Methanol	$1 - \frac{M(t)}{M_0} = 0.23 \bullet \sqrt{t}$	0.978
	Ethanol	$1 - \frac{M(t)}{M_0} = 0.23 \bullet \sqrt{t}$	0.985
	2-Propanol	$1 - \frac{M(t)}{M_0} = 0.19 \bullet \sqrt{t}$	0.955

force of the mass release may be associated with the advective flow:

$$\frac{\partial C}{\partial t} = -v \bullet \frac{\partial C}{\partial x}, \tag{4}$$

where v is the drift velocity (m/s). The solution of this equation admits linear evolution of the diffusing substance mass versus time [57]:

$$\frac{M(t)}{M_0} = 1 - \frac{v}{L} \bullet t. \tag{5}$$

Figure 8 demonstrates the experimental data at small times fitted by equation (5). A good correspondence between the experimental data and the theoretical solution is observed. The measured fitting parameters are listed in Table 2. The fitted slopes increase in the following order: 2-propanol > methanol > ethanol. This situation holds for the mass release from either individual MWCNTs or MWCNT bundles. The mass release from the MWCNT bundles exhibits higher v/L values than that from the individual MWCNTs. The mass release is controlled by the advective mechanism in the $M(t)/M_0$ range of 0.5–1, i.e. at small times. Therefore, the crossover between small and long times occurs at $M(t)/M_0 = 0.5$. This is in good agreement with the findings obtained in Ref. [58]. According to Figure 6, the crossover time is nearly 5–6 s.

3.2.3. Long-Time Analysis. In the frame of the second Fick's law, the mass release is proportional to the square root of time at small times, whereas at long times, the mass decay follows an exponential trend versus time, as it is theoretically established by Zel'dovich and Myshkis [59]. The relevant solution may be given by the following:

$$\frac{M(t)}{M_0} = A \bullet \exp\left[-\frac{D \bullet \pi^2 \bullet t}{L^2}\right]. \tag{6}$$

Here, A is a coefficient defined by the initial and boundary conditions and by the geometry of a medium where the diffusion occurs. Coefficient A may equal $6/\pi^2$, $8/\pi^2$, $32/\pi^2$, etc. [60].

For the experimental data analysis, the solution of the diffusion equation in exponential form is usually linearized in semilogarithmic coordinates [61]:

$$\ln\left[\frac{M(t)}{M_0}\right] = \ln[A] - \frac{D \bullet \pi^2}{L^2} \bullet t. \tag{7}$$

Taking the logarithm of equation (7) yields the following:

$$\ln\left[\ln[A] - \ln\left[\frac{M(t)}{M_0}\right]\right] = \ln\left[\frac{D \bullet \pi^2}{L^2}\right] + \ln[t]. \tag{8}$$

The slope in equation (8) equals unity. Therefore, the bi-log-log plot of the experimental data should be characterized by the slope identical to unity. Deviation of the experimental slope from unity may provide evidence of anomalous diffusion kinetics. In the experimental scenario, transport of all alcohols from either individual MWCNTs or MWCNT bundles experiences standard Fickian behavior. The log of $M(t)/M_0$ plotted against time provides a linear function (Figure 9). The bi-log of the experimental alcohol release is fairly linear versus the time log (Figure 10), whereas the slopes of the logarithmically transformed experimental data are almost identical to unity (Table 3).

3.3. Estimation of the Mass Transfer Parameters. The diffusion coefficient may be estimated using the slope in equation (7). According to equation (7), the fitted value of the slope is related to the diffusion coefficient as follows: slope $= D \times \pi^2/L^2$. Drift velocity is evaluated from the slope in equation (5). To calculate the diffusion coefficient and drift velocity, knowledge about the diffusion length is required. The typical size of the MWCNT bundle is approximately 4 μm (Figure 2(a)), whereas the mean

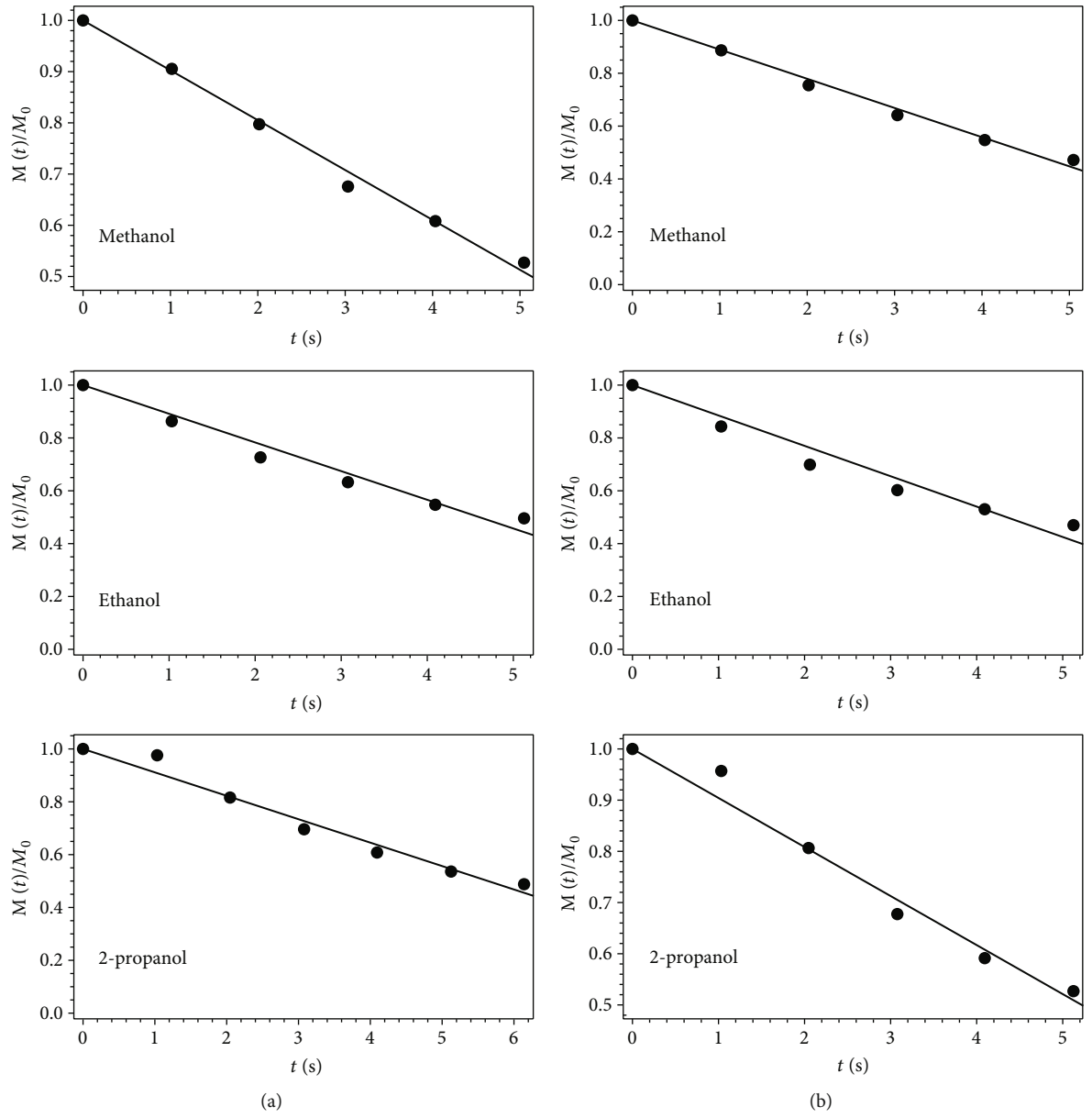

Figure 8: Experimental data (points) fitted by equation (5) (solid line) for individual MWCNTs (a) and MWCNT bundles (b).

length of the individual MWCNTs is about $1.6\,\mu$m (Figure 2(b)). However, the diffusion length may be larger than the size of the corresponding nanotube object. The diffusing species may move from one nanotube to another. Accounting for TEM images, the diffusion length may be up to 3 times larger due to the contacts between the nanotubes for the individual MWCNTs. For the MWCNT bundles, the diffusion length is scarcely considerably larger than the size of the bundle because the nanotubes in a bundle are characterized by a large number of contacts. Therefore, the diffusion lengths are $L = 3 \times 1.6 \times 10^{-6} = 4.8 \times 10^{-6}$ m and $L = 4 \times 10^{-6}$ m for the individual MWCNTs and MWCNT bundles, respectively.

The estimated mass transfer parameters are listed in Table 4. Irrespectively to the PQR coating, the highest drift velocity is observed for ethanol, whereas 2-propanol transport is characterized by the lowest drift velocity. For both PQR coatings, the diffusion coefficient decreases in the following order: methanol > ethanol > 2-propanol. Both bulk and surface diffusivities strongly depend on the molecular weight of the diffusing substance [62]. An identical situation is observed in the experimental scenario studied. The obtained mass transfer parameters are very similar for both coatings. However, the values of the diffusion coefficients are several orders of magnitude different compared to the data reported for CNTs. In particular, the self-diffusion coefficient of CO_2 and CH_4 in CNTs and CNT bundles estimated from molecular simulations was of the order of 10^{-8} m^2/s [22]. In the MWCNTs with the inner diameter of 6.7 ± 0.8 nm, the effective self-diffusion coefficient of the

Table 2: Fitting results from Figure 8.

Figure	Alcohol	Fitted equation	R^2
Figure 8(a)	Methanol	$\frac{M(t)}{M_0} = 1 - 0.097 \bullet t$	0.992
	Ethanol	$\frac{M(t)}{M_0} = 1 - 0.108 \bullet t$	0.963
	2-Propanol	$\frac{M(t)}{M_0} = 1 - 0.089 \bullet t$	0.970
Figure 8(b)	Methanol	$\frac{M(t)}{M_0} = 1 - 0.110 \bullet t$	0.990
	Ethanol	$\frac{M(t)}{M_0} = 1 - 0.115 \bullet t$	0.945
	2-Propanol	$\frac{M(t)}{M_0} = 1 - 0.096 \bullet t$	0.976

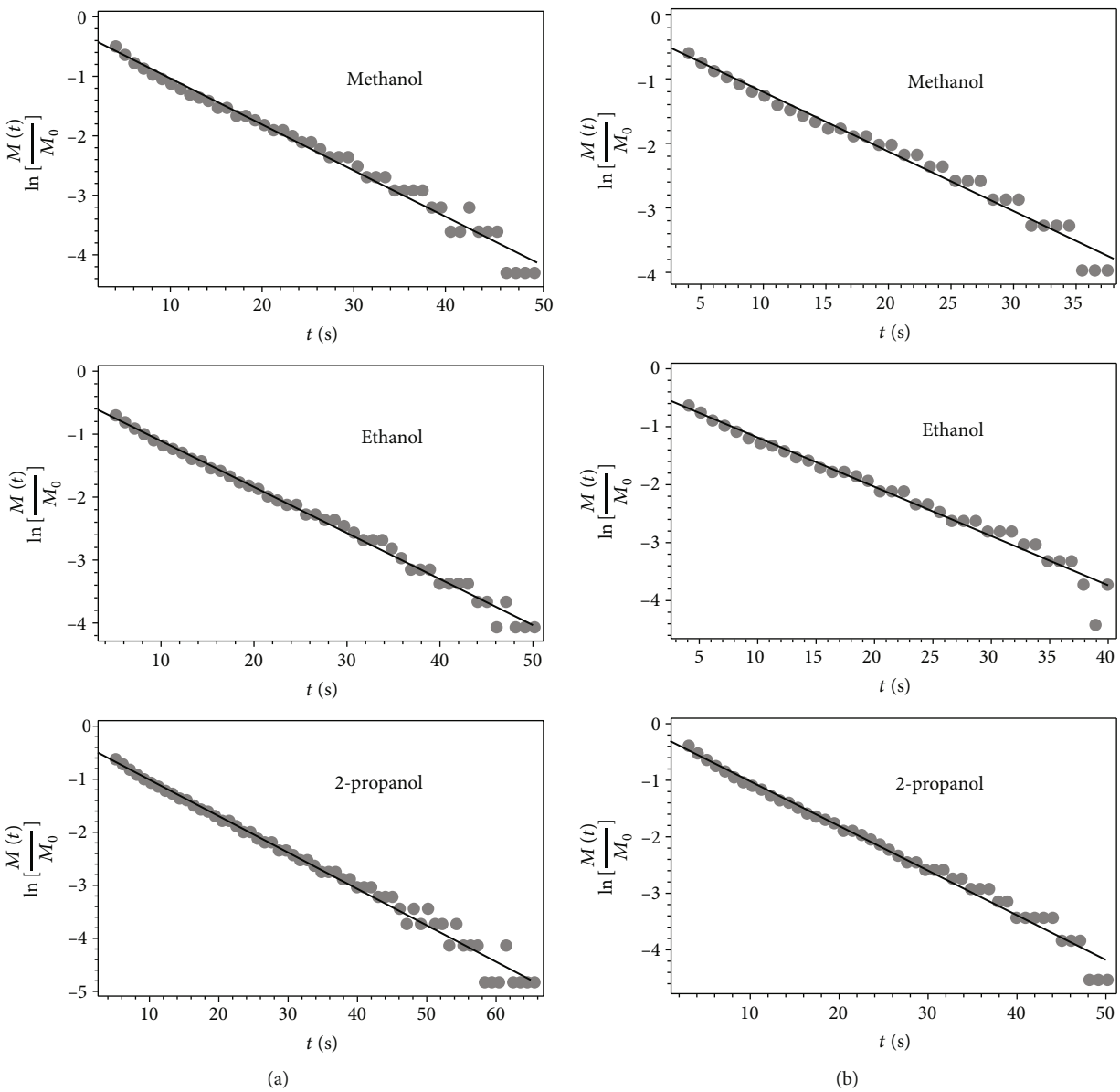

Figure 9: Semilog plots of the experimental data (points) fitted by equation (7) (solid lines) for individual MWCNTs (a) and MWCNT bundles (b).

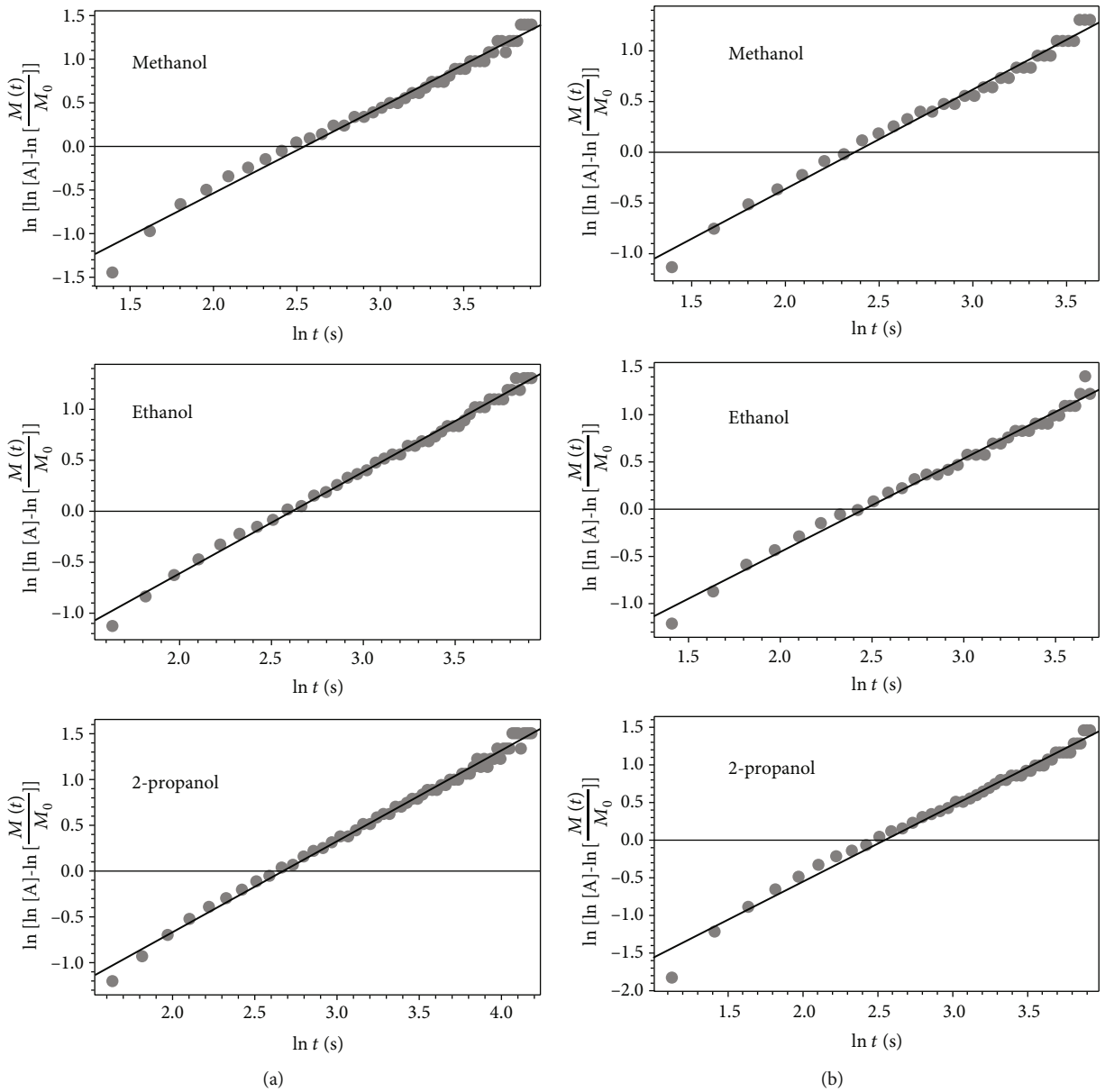

Figure 10: Log-log plots of the experimental data (points) and fittings based on equation (8) (solid lines) for individual MWCNTs (a) and MWCNT bundles (b).

water studied by PFG NMR was equal to 10^{-10} m^2/s [33]. The molecular dynamics simulations revealed that the water self-diffusivity in CNTs was 10^{-9} m^2/s [23, 63]. The latter value was also obtained for ions diffusion through CNTs [64]. The published data concern the diffusion inside the CNTs. The MWCNTs used in this study are mainly closed from both ends so that the diffusing molecules can scarcely reach the internal space of the MWCNTs. Therefore, the mass release is seemingly controlled by the diffusion of the alcohol molecules on the surface of the MWCNTs. The retention time is defined by the time of the alcohol residence on the MWCNT surface. In this case, the diffusion length is equal to the distance traveled by the molecules on the MWCNT surface. It should be emphasized that duplicating the experiments yields the deviation of the slope in equation (8) less than 5%. This affects only the digit in the third decimal place for the measured value of D. Since the value of D is rounded to two decimals (Table 4), the effects of variability and errors are too small to affect the obtained results.

The diffusivities estimated from the experiment are quite similar to the reported values of the surface diffusion coefficients on carbon materials. Surface diffusion coefficients of various organic chemicals on activated carbon were found to be in the range of 10^{-13}–10^{-10} m^2/s [65–67]. The surface diffusion coefficient of ethanol on activated carbon is 10^{-11} m^2/s [62]. For solid-phase

Table 3: Fitting results from Figures 9 and 10.

Figure	Alcohol	Fitted equation	R^2
Figure 9(a)	Methanol	$\ln\left[\frac{M(t)}{M_0}\right] = -0.26 - 0.077 \bullet t$	0.981
	Ethanol	$\ln\left[\frac{M(t)}{M_0}\right] = -0.38 - 0.073 \bullet t$	0.993
	2-Propanol	$\ln\left[\frac{M(t)}{M_0}\right] = -0.32 - 0.069 \bullet t$	0.985
Figure 9(b)	Methanol	$\ln\left[\frac{M(t)}{M_0}\right] = -0.28 - 0.092 \bullet t$	0.978
	Ethanol	$\ln\left[\frac{M(t)}{M_0}\right] = -0.34 - 0.085 \bullet t$	0.971
	2-Propanol	$\ln\left[\frac{M(t)}{M_0}\right] = -0.23 - 0.079 \bullet t$	0.984
Figure 10(a)	Methanol	$\ln\left[\ln[A] - \ln\left[\frac{M(t)}{M_0}\right]\right] = -2.50 + 0.98 \bullet \ln t$	0.986
	Ethanol	$\ln\left[\ln[A] - \ln\left[\frac{M(t)}{M_0}\right]\right] = -2.60 + 1.00 \bullet \ln t$	0.995
	2-Propanol	$\ln\left[\ln[A] - \ln\left[\frac{M(t)}{M_0}\right]\right] = -2.65 + 0.99 \bullet \ln t$	0.994
Figure 10(b)	Methanol	$\ln\left[\ln[A] - \ln\left[\frac{M(t)}{M_0}\right]\right] = -2.32 + 0.98 \bullet \ln t$	0.988
	Ethanol	$\ln\left[\ln[A] - \ln\left[\frac{M(t)}{M_0}\right]\right] = -2.43 + 0.99 \bullet \ln t$	0.989
	2-Propanol	$\ln\left[\ln[A] - \ln\left[\frac{M(t)}{M_0}\right]\right] = -2.57 + 1.01 \bullet \ln t$	0.988

Table 4: Measured mass transfer parameters.

PQR coating	Alcohol	$D \times 10^{13}$ (m^2/s)	$v \times 10^7$ (m/s)
Individual MWCNTs	Methanol	1.80	4.66
	Ethanol	1.70	5.18
	2-Propanol	1.61	4.27
MWCNT bundles	Methanol	1.49	4.40
	Ethanol	1.38	4.60
	2-Propanol	1.28	3.84

diffusion of acid dyes on activated carbon, the diffusion coefficients in the range of 10^{-15}–10^{-14} m^2/s were reported [68].

To the best of our knowledge, this is the first experimental result concerning the diffusion of C_1–C_3 alcohols over carbon nanotubes. Due to the lack of adequate experimental background in the literature, it is challenging to judge whether the obtained diffusivities are comparable with the surface diffusivities on carbon nanomaterials, e.g., CNTs. The reported diffusion coefficients in CNTs range between 10^{-10} m^2/s and 10^{-8} m^2/s. The surface diffusivities obtained in this study are of the order 10^{-13} m^2/s. Three orders of magnitude inequality between the diffusivities inside CNTs and the diffusivities on the surface of CNTs may be convenient. For example, in coal, the pore diffusivity is nearly two orders of magnitude higher than the surface diffusivity [69].

4. Conclusions

Many studies indicate deviations from Fick's law in CNTs. Enhanced transport of some molecules, mainly water, in CNTs has also been reported. In this study, no evidence of ultrafast transport of C_1–C_3 alcohols on the surface of the individual MWCNTs and MWCNT bundles has been found. The experimental diffusion kinetics follows the second Fick's law in a precise manner at long times, whereas advective transport is identified at small times. The

measured surface diffusion coefficients and drift velocities are in the order of 10^{-13} m^2/s and 10^{-7} m/s, respectively. The obtained diffusivity values reveal that the diffusion rate is not "enhanced."

Data Availability

The data supporting the conclusions of the study may be obtained from the corresponding author upon a reasonable request.

Disclosure

This work was completed despite the unprovoked invasion of Ukraine by Russia, supported by Belarus. Funds originally granted by the NRFU were partially diverted, by a resolution of the Cabinet of Ministers of Ukraine, to defend Ukraine against the Russian invasion.

Conflicts of Interest

The authors declare no conflict of interest.

Acknowledgments

The authors are thankful to the Armed Forces of Ukraine for serving our country and protecting our freedoms. The authors are thankful to P. S. Yaremov for his help in recording and interpreting the adsorption-desorption isotherms. This research received funding from the National Research Foundation of Ukraine (NRFU, grant 2020.02/0050).

References

[1] M. Miao, "Electrical conductivity of pure carbon nanotube yarns," *Carbon*, vol. 49, no. 12, pp. 3755–3761, 2011.

[2] Á. Kukovecz, G. Kozma, and Z. Kónya, "Multi-walled carbon nanotubes," in *Springer Handbook of Nanomaterials*, pp. 147–188, Springer Berlin Heidelberg, 2013.

[3] B. Kumanek and D. Janas, "Thermal conductivity of carbon nanotube networks: a review," *Journal of Materials Science*, vol. 54, no. 10, pp. 7397–7427, 2019.

[4] A. Eatemadi, H. Daraee, H. Karimkhanloo et al., "Carbon nanotubes: properties, synthesis, purification, and medical applications," *Nanoscale Research Letters*, vol. 9, no. 1, p. 393, 2014.

[5] E. Bekyarova, Y. Ni, E. B. Malarkey et al., "Applications of carbon nanotubes in biotechnology and biomedicine," *Journal of Biomedical Nanotechnology*, vol. 1, no. 1, pp. 3–17, 2005.

[6] G. Rahman, Z. Najaf, A. Mehmood et al., "An overview of the recent progress in the synthesis and applications of carbon nanotubes," *Journal of Carbon Research*, vol. 5, no. 1, p. 3, 2019.

[7] J. M. Schnorr and T. M. Swager, "Emerging applications of carbon nanotubes," *Chemistry of Materials*, vol. 23, no. 3, pp. 646–657, 2011.

[8] S. Abdalla, F. Al-Marzouki, A. A. Al-Ghamdi, and A. Abdel-Daiem, "Different technical applications of carbon nanotubes," *Nanoscale Research Letters*, vol. 10, no. 1, p. 358, 2015.

[9] S. M. Fatemi and M. Foroutan, "Review on carbon nanotubes and carbon nanotube bundles for gas/ion separation and water purification studied by molecular dynamics simulation," *International journal of Environmental Science and Technology*, vol. 13, no. 2, pp. 457–470, 2016.

[10] T. Araki, R. Cruz-Silva, S. Tejima et al., "Water diffusion mechanism in carbon nanotube and polyamide nanocomposite reverse osmosis membranes: a possible percolation-hopping mechanism," *Physical Review Applied*, vol. 9, no. 2, article 024018, 2018.

[11] M. T. Bankole, A. S. Abdulkareem, I. A. Mohammed et al., "Selected heavy metals removal from electroplating wastewater by purified and polyhydroxylbutyrate functionalized carbon nanotubes adsorbents," *Scientific Reports*, vol. 9, no. 1, p. 4475, 2019.

[12] A. Ihsanullah, A. M. Abbas, T. Al-Amer et al., "Heavy metal removal from aqueous solution by advanced carbon nanotubes: critical review of adsorption applications," *Separation and Purification Technology*, vol. 157, pp. 141–161, 2016.

[13] D. Zacs, I. Rozentale, I. Reinholds, and V. Bartkevics, "Multi-walled carbon nanotubes as effective sorbents for rapid analysis of polycyclic aromatic hydrocarbons in edible oils using dispersive solid-phase extraction (d-SPE) and gas chromatography—tandem mass spectrometry (GC-MS/MS)," *Food Analytical Methods*, vol. 11, no. 9, pp. 2508–2517, 2018.

[14] K. Pyrzynska, "Carbon nanotubes as sorbents in the analysis of pesticides," *Chemosphere*, vol. 83, no. 11, pp. 1407–1413, 2011.

[15] B. Socas-Rodríguez, A. V. Herrera-Herrera, M. Asensio-Ramos, and J. Hernández-Borges, "Recent applications of carbon nanotube sorbents in analytical chemistry," *Journal of Chromatography. A*, vol. 1357, pp. 110–146, 2014.

[16] Y. Yan, J. Miao, Z. Yang et al., "Carbon nanotube catalysts: recent advances in synthesis, characterization and applications," *Chemical Society Reviews*, vol. 44, no. 10, pp. 3295–3346, 2015.

[17] L. M. Esteves, H. A. Oliveira, and F. B. Passos, "Carbon nanotubes as catalyst support in chemical vapor deposition reaction: a review," *Journal of Industrial and Engineering Chemistry*, vol. 65, pp. 1–12, 2018.

[18] M. F. R. Pereira, J. L. Figueiredo, J. J. M. Órfão, P. Serp, P. Kalck, and Y. Kihn, "Catalytic activity of carbon nanotubes in the oxidative dehydrogenation of ethylbenzene," *Carbon*, vol. 42, no. 14, pp. 2807–2813, 2004.

[19] Y. N. Zhitnev, E. A. Tveritinova, S. A. Chernyak, S. V. Savilov, and V. V. Lunin, "Catalytic activity of carbon nanotubes in the conversion of aliphatic alcohols," *Russian Journal of Physical Chemistry A*, vol. 90, no. 6, pp. 1128–1131, 2016.

[20] I. Bychko and P. Strizhak, "Carbon nanotubes catalytic activity in the ethylene hydrogenation," *Fullerenes, Nanotubes, and Carbon Nanostructures*, vol. 26, no. 12, pp. 804–809, 2018.

[21] B.-H. Chen, C. Kung, and I.-P. Chu, "Mechanisms of hydrogen transport in flexible-wall narrow carbon nanotubes," *Journal of Nanomaterials*, vol. 2015, Article ID 959402, 10 pages, 2015.

[22] W. Cao, G. M. Tow, L. Lu, L. Huang, and X. Lu, "Diffusion of CO_2/CH_4 confined in narrow carbon nanotube bundles," *Molecular Physics*, vol. 114, no. 16-17, pp. 2530–2540, 2016.

[23] A. Barati Farimani and N. R. Aluru, "Spatial diffusion of water in carbon nanotubes: from Fickian to ballistic motion," *The Journal of Physical Chemistry. B*, vol. 115, no. 42, pp. 12145–12149, 2011.

[24] R. Krishna and J. M. Van Baten, "Describing binary mixture diffusion in carbon nanotubes with the Maxwell-Stefan equations. An investigation using molecular dynamics

simulations," *Industrial & Engineering Chemistry Research*, vol. 45, pp. 2084–2093, 2006.

[25] S. Yeganegi and F. Gholampour, "Simulation of methane adsorption and diffusion in a carbon nanotube channel," *Chemical Engineering Science*, vol. 140, pp. 62–70, 2016.

[26] Z. Hu, H. Xie, Q. Wang, and S. Chen, "Adsorption and diffusion of sulfur dioxide and nitrogen in single-wall carbon nanotubes," *Journal of Molecular Graphics & Modelling*, vol. 88, pp. 62–70, 2019.

[27] J. Feng, P. Chen, D. Zheng, and W. Zhong, "Transport diffusion in deformed carbon nanotubes," *Physica A: Statistical Mechanics and its Applications*, vol. 493, pp. 155–161, 2018.

[28] A. Striolo, "The mechanism of water diffusion in narrow carbon nanotubes," *Nano Letters*, vol. 6, no. 4, pp. 633–639, 2006.

[29] A. Parmentier, M. Maccarini, A. De Francesco et al., "Neutron spin echo monitoring of segmental-like diffusion of water confined in the cores of carbon nanotubes," *Physical Chemistry Chemical Physics*, vol. 21, no. 38, pp. 21456–21463, 2019.

[30] Y. Zheng, H. Ye, Z. Zhang, and H. Zhang, "Water diffusion inside carbon nanotubes: mutual effects of surface and confinement," *Physical Chemistry Chemical Physics*, vol. 14, no. 2, pp. 964–971, 2012.

[31] B. H. S. Mendonça, D. N. de Freitas, M. H. Köhler, R. J. C. Batista, M. C. Barbosa, and A. B. de Oliveira, "Diffusion behaviour of water confined in deformed carbon nanotubes," *Physica A: Statistical Mechanics and its Applications*, vol. 517, pp. 491–498, 2019.

[32] A. Ghoufi, A. Szymczyk, and P. Malfreyt, "Ultrafast diffusion of ionic liquids confined in carbon nanotubes," *Scientific Reports*, vol. 6, no. 1, article 28518, 2016.

[33] X. Liu, X. Pan, S. Zhang, X. Han, and X. Bao, "Diffusion of water inside carbon nanotubes studied by pulsed field gradient NMR spectroscopy," *Langmuir*, vol. 30, no. 27, pp. 8036–8045, 2014.

[34] J. J. Castillo, M. H. Torres, D. R. Molina et al., "Monitoring the functionalization of single-walled carbon nanotubes with chitosan and folic acid by two-dimensional diffusion-ordered NMR spectroscopy," *Carbon*, vol. 50, pp. 2691–2697, 2012.

[35] G. Briganti, G. Rogati, A. Parmentier, M. Maccarini, and F. De Luca, "Neutron scattering observation of quasi-free rotations of water confined in carbon nanotubes," *Scientific Reports*, vol. 7, no. 1, article 45021, 2017.

[36] S. C. Lim, K. Kang Kim, S. Hun Jeong, K. Hyeok An, S.-B. Lee, and Y. H. Lee, "Dual quartz crystal microbalance for hydrogen storage in carbon nanotubes," *International Journal of Hydrogen Energy*, vol. 32, no. 15, pp. 3442–3447, 2007.

[37] Y. Zhang, K. Yu, R. Xu, D. Jiang, L. Luo, and Z. Zhu, "Quartz crystal microbalance coated with carbon nanotube films used as humidity sensor," *Sensors and Actuators A: Physical*, vol. 120, no. 1, pp. 142–146, 2005.

[38] E. S. Mañoso, R. Herrera-Basurto, B. M. Simonet, and M. Valcárcel, "A quartz crystal microbalance modified with carbon nanotubes as a sensor for volatile organic compounds," *Sensors and Actuators B: Chemical*, vol. 186, pp. 811–816, 2013.

[39] P. M. Lutsyk, P. Shankar, A. G. Rozhin, and S. A. Kulinich, "Surface sensitivity of ultrasonically treated carbon nanotube network towards ammonia," *Surfaces and Interfaces*, vol. 17, article 100363, 2019.

[40] B. Pejcic, M. Myers, N. Ranwala, L. Boyd, M. Baker, and A. Ross, "Modifying the response of a polymer-based quartz crystal microbalance hydrocarbon sensor with functionalized carbon nanotubes," *Talanta*, vol. 85, no. 3, pp. 1648–1657, 2011.

[41] H. Tai, X. Bao, Y. He, X. Du, G. Xie, and Y. Jiang, "Enhanced formaldehyde-sensing performances of mixed polyethyleneimine-multiwalled carbon nanotubes composite films on quartz crystal microbalance," *IEEE Sensors Journal*, vol. 15, no. 12, pp. 6904–6911, 2015.

[42] P. Yi and K. L. Chen, "Release kinetics of multiwalled carbon nanotubes deposited on silica surfaces: quartz crystal microbalance with dissipation (QCM-D) measurements and modeling," *Environmental Science & Technology*, vol. 48, no. 8, pp. 4406–4413, 2014.

[43] U. Burghaus, D. Bye, K. Cosert et al., "Methanol adsorption in carbon nanotubes," *Chemical Physics Letters*, vol. 442, no. 4-6, pp. 344–347, 2007.

[44] S. C. Hsu and C. Lu, "Adsorption kinetic, thermodynamic, and desorption studies of isopropyl alcohol vapor by oxidized single-walled carbon nanotubes," *Journal of the Air & Waste Management Association (1995)*, vol. 59, no. 8, pp. 990–997, 2009.

[45] S.-J. Young and Z.-D. Lin, "Ethanol gas sensors composed of carbon nanotubes with au nanoparticles adsorbed onto a flexible PI substrate," *ECS Journal of Solid State Science and Technology*, vol. 6, no. 10, pp. M130–M132, 2017.

[46] L. Lu, Q. Shao, L. Huang, and X. Lu, "Simulation of adsorption and separation of ethanol-water mixture with zeolite and carbon nanotube," *Fluid Phase Equilibria*, vol. 261, no. 1-2, pp. 191–198, 2007.

[47] A. Simion, A. Pîrnău, F. R. V. Turcu et al., "Stratified diffusion of HOD-D_2O inside COOH- and NH_2-functionalized multi-walled carbon nanotubes studied by NMR spectroscopy," *Journal of Molecular Structure*, vol. 1249, article 131653, 2022.

[48] Q. Wang, L. Liu, C. Liu, J. Song, and X. Gao, "Size effect in determining the water diffusion rate in carbon nanotubes," *Journal of Molecular Liquids*, vol. 334, article 116034, 2021.

[49] N. V. Lemesh, A. I. Tripol'skii, I. E. Kotenko, V. A. Khavrus, and P. E. Strizhak, "Structural parameters of carbon nanotubes obtained by the chemical vapor decomposition of ethylene onto nickel nanoparticles deposited on basic supports," *Theoretical and Experimental Chemistry*, vol. 46, pp. 296–301, 2010.

[50] I. B. Bychko, A. A. Abakumov, N. V. Lemesh, and P. E. Strizhak, "Catalytic activity of multiwalled carbon nanotubes in acetylene hydrogenation," *ChemCatChem*, vol. 9, no. 24, pp. 4470–4474, 2017.

[51] A. P. Filippov, "The possibilities of applying QCM method in pulsed mode for investigating the adsorption dynamics of volatile compounds on finely dispersed sorbents," *Adsorption Science and Technology*, vol. 30, no. 5, pp. 425–436, 2012.

[52] K. S. W. Sing and R. T. Williams, "Physisorption hysteresis loops and the characterization of nanoporous materials," *Adsorption Science and Technology*, vol. 22, no. 10, pp. 773–782, 2004.

[53] N. K. Nadermann, E. P. Chan, and C. M. Stafford, "Bilayer mass transport model for determining swelling and diffusion in coated, ultrathin membranes," *ACS Applied Materials & Interfaces*, vol. 7, no. 6, pp. 3492–3502, 2015.

[54] S. Brandani and D. M. Ruthven, "Analysis of ZLC desorption curves for gaseous systems," *Adsorption*, vol. 2, no. 2, pp. 133–143, 1996.

[55] B. Sakintuna, E. Fakioglu, and Y. Yürüm, "Diffusion of volatile organic chemicals in porous media. 1. Alcohol/natural zeolite systems," *Energy & Fuels*, vol. 19, pp. 2219–2224, 2005.

[56] B. Sakintuna, Y. Yurum, and O. Cuhadar, "Diffusion of volatile organic chemicals in porous media. 2. Alcohol/templated porous carbon systems," *Energy & Fuels*, vol. 20, pp. 1269–1274, 2006.

[57] A. Zhokh and P. Strizhak, "Advection–diffusion in a porous medium with fractal geometry: fractional transport and cross-overs on time scales," *Meccanica*, vol. 57, no. 4, pp. 833–843, 2022.

[58] J. Y. Liu and W. T. Simpson, "Solutions of diffusion equation with constant diffusion and surface emission coefficients," *Drying Technology*, vol. 15, no. 10, pp. 2459–2477, 1997.

[59] Y. B. Zel'dovich and A. D. Myshkis, *Elements of Mathematical Physics [in Russian]*, Nauka Publishing House, Moscow, Russia, 1973.

[60] N. Malekjani and S. M. Jafari, "Modeling the release of food bioactive ingredients from carriers/nanocarriers by the empirical, semiempirical, and mechanistic models," *Comprehensive Reviews in Food Science and Food Safety*, vol. 20, no. 1, pp. 3–47, 2021.

[61] D. M. Ruthven and A. Vidoni, "ZLC diffusion measurements: combined effect of surface resistance and internal diffusion," *Chemical Engineering Science*, vol. 71, pp. 1–4, 2012.

[62] D. D. Do and H. D. Do, "Surface diffusion of hydrocarbons in activated carbon: comparison between constant molar flow, differential permeation and differential adsorption bed methods," *Adsorption*, vol. 7, pp. 189–209, 2001.

[63] X. Gao, T. Zhao, and Z. Li, "Effects of ions on the diffusion coefficient of water in carbon nanotubes," *Journal of Applied Physics*, vol. 116, no. 5, article 054311, 2014.

[64] S. F. Buchsbaum, M. L. Jue, A. M. Sawvel et al., "Fast permeation of small ions in carbon nanotubes," *Advancement of Science*, vol. 8, no. 3, article 2001802, 2021.

[65] U. K. Traegner and M. T. Suidan, "Evaluation of surface and film diffusion coefficients for carbon adsorption," *Water Research*, vol. 23, no. 3, pp. 267–273, 1989.

[66] S. Baup, D. Wolbert, and A. Laplanche, "Importance of surface diffusivities in pesticide adsorption kinetics onto granular versus powdered activated carbon: experimental determination and modeling," *Environmental Technology*, vol. 23, no. 10, pp. 1107–1117, 2002.

[67] M. Suzuki and K. Kawazoe, "Effective surface diffusion coefficients of volatile organics on activated carbon during adsorption from aqueous solution," *Journal of Chemical Engineering of Japan*, vol. 8, no. 5, pp. 379–382, 1975.

[68] K. K. H. Choy, J. F. Porter, and G. McKay, "Film-surface diffusion during the adsorption of acid dyes onto activated carbon," *Journal of Chemical Technology and Biotechnology*, vol. 79, no. 11, pp. 1181–1188, 2004.

[69] C. Ö. Karacan and G. D. Mitchell, "Behavior and effect of different coal microlithotypes during gas transport for carbon dioxide sequestration into coal seams," *International Journal of Coal Geology*, vol. 53, no. 4, pp. 201–217, 2003.